https://arabjchem.org

ScientificScholar®
Knowledge is power
Publisher of Scientific Journals

Arabian Journal of Chemistry

2026 19 (2) 6052025

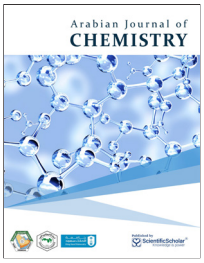

Original Article

Impact of acidic and oxidative environments on layer-by-layer membranes for vanadium redox flow batteries: Stability and degradation

Saidatul Sophia Sha'rani[a,b], Eleen Dayana Mohamed Isa[a], Noor Fatina Emelin Nor Fadzil[a], Mohamed Mahmoud Nasef[a,b], Ebrahim Abouzari-Lotf[c,d], Nurfatehah Wahyuny Che Jusoh[a,b*]

[a]*Department of Chemical and Environmental Engineering (ChEE), Malaysia–Japan International Institute of Technology, Universiti Teknologi Malaysia, Kuala Lumpur, Malaysia*
[b]*Advanced Materials Research Group, Center of Hydrogen Energy (CHE), Universiti Teknologi Malaysia, Kuala Lumpur, Malaysia*
[c]*Helmholtz Institute Ulm (HIU) Electrochemical Energy Storage, Helmholtzstraße 11, Germany Institute of Nanotechnology, Karlsruhe Institute of Technology (KIT), Hermann-von-Helmholtz-Platz 1, Eggenstein-Leopoldshafen, Germany*

ARTICLE INFO

Keywords:
Acidic & oxidative stability
Degradation mechanism
Layer-by-layer membrane
Vanadium redox flow battery

ABSTRACT

The layer-by-layer (LbL) assembly technique has emerged as a versatile and cost-effective method for surface modification, gaining significant widespread attention across various applications. This study evaluates the physicochemical and electrochemical properties of Nafion-based LbL membranes, N117-(PEI/GO)*n*, incorporating polyethylenimine (PEI) and graphene oxide (GO), and their stability in acidic and oxidative environments of vanadium redox flow battery (VRFB) catholytes. The LbL membranes were subjected to normal (0.1 M VO_2^+ in 3.0 M H_2SO_4) and accelerated (1.5 M VO_2^+ in 3.0 M H_2SO_4) degradation for 60 days. Analysis revealed notable changes in the physicochemical properties, with diminished peaks for PEI and GO in the Fourier-transform infrared (FTIR) spectrum and weight loss up to 9.9%. Raman spectroscopy further supported these findings, showing a reduction in the intensity of the characteristic D and G bands, which indicates partial degradation of the GO layers after immersion, particularly under accelerated conditions. Meanwhile, the electrochemical properties exhibited significant changes in ion exchange capacity (IEC), which increased by 7%, proton conductivity rose by 41%, and vanadium permeability increased by 762% under accelerated conditions. These changes were attributed to the hydrolysis and oxidation of PEI and GO, driven by highly oxidizing VO_2^+ ions and acidic conditions, which weakened electrostatic and chemical interactions in the LbL structure. A plausible degradation mechanism was proposed to illustrate the membrane degradation behavior, along with several potential strategies to enhance membrane performance in VRFB operation.

1. Introduction

The layer-by-layer (LbL) assembly technique has garnered significant attention due to its versatility and cost-effectiveness in modifying substrate surfaces. Initially demonstrated by Iller in 1966 using colloid particles [1] and later expanded upon by Decher using polyelectrolytes (PEs) [2], this method has found extensive applications in various fields, including biomedicine [3], biosensors [4], desalination [5], agricultural waste [6,7], and membrane separation [8-11]. The LbL method involves the alternate immersions of substrate in polycation and polyanion solutions followed by rinsing with water to remove excessive PEs and rearrange the adsorbed PE layers [5]. This method allows precise control over the composition, stability, porosity, and surface functionalities of the membranes through various interactions such as electrostatic forces, hydrogen bonding, and van der Waals interactions [12].

In the context of vanadium redox flow batteries (VRFBs), LbL membranes have been widely studied for their potential to reduce vanadium permeability and enhance battery performance. Commonly employed PEs for LbL membranes in VRFBs include poly (diallyldimethylammonium chloride) (PDDA) as the polycations and poly (sodium styrene sulfonate) (PSS) as the polyanions, forming PDDA/PSS bilayers [13-17]. Other combinations have also been explored, including PDDA/Zirconium phosphate (ZrP) [18], azide-containing quaternary ammonium polystyrene/sulfonated poly(2,6-dimethyl-1,4-phenylene oxide) (amPS-az/sPPO) [19], chitosan/phosphotungstic acid (CS/PWA) [20], and PDDA/Nafion [21]. Despite promising results in reducing vanadium permeability and improving coulombic efficiency (CE) and durability, many studies have highlighted limitations in the cycle counts, emphasizing the need for comprehensive in-situ and ex-situ stability testing to fully understand the long-term stability of these membranes. Practically, in-situ evaluation through VRFB cycling and monitoring changes in the membrane properties is time-consuming due to the lengthy charge-discharge process of liquid flow batteries. Therefore, the ex-situ stability testing method, which involves immersing the membrane in VRFB catholyte, is preferred as it expedites the test and provides qualitative insights into the oxidative stability of the membrane [22].

Branched polyethylenimine (PEI) has been extensively studied for its unique properties, making it an excellent candidate for LbL assemblies. PEI, a cationic polymer with a high density of amine groups, facilitates strong electrostatic interactions with negatively charged species [23-

***Corresponding author:**
E-mail address: nurfatehah@utm.my (N.W.C. Jusoh)

Received: 28 May, 2025 **Accepted:** 01 November, 2025 **Epub Ahead of Print:** 07 January, 2026 **Published:** 02 February, 2026
DOI: 10.25259/AJC_605_2025

26]. This high charge density enhances the binding strength in LbL assemblies and contributes to the mechanical robustness and chemical stability of the resulting membranes. In vanadium/air redox flow batteries (VARFBs), PEI has been paired with Nafion to form (PEI/Nafion) membranes, demonstrating an increase in selectivity by a factor of 21. Additionally, PEI/Graphene oxide (GO) bilayers have shown promising results in applications like pervaporation [23], desalination [27-29], and surface coatings [30,31]. GO, which contains carboxyl groups, exhibits a negative charge, making it a suitable candidate as a polyanion for LbL assembly [32,33]. The use of GO as a polyanion in LbL membranes for VRFBs has yet to be thoroughly explored. GO offers strong stability in acidic environments; thus, incorporating GO as a polyanion could enhance membrane stability, as GO can effectively restrict the migration of PE chains [28,34].

Recently, extensive efforts have been dedicated to enhancing the stability of LbL membranes for use in VRFBs. Studies have demonstrated that the choice of PEs and their binding strength play crucial roles in determining the long-term performance of these membranes. For instance, LbL membranes incorporating Nafion (N117)-based substrates, modified with PEI/GO bilayers, have shown promising results. Notably, N117-(PEI/GO)n membranes exhibit excellent stability over more than 100 cycles at a current density of 40 $mA.cm^{-2}$, demonstrating the effectiveness of LbL modification [35]. Despite these advancements, the stability of PEI in the highly acidic and oxidative VRFB environment remains a significant limitation [36].

The VRFB environment, characterized by concentrated acidic conditions (2.0 – 4.0 M) and oxidative stress due to vanadium species, imposes severe challenges on membrane materials. These challenges include fouling, erosion, swelling, and loss of chemical and mechanical integrity, all of which can severely compromise membrane performance [37,38]. The effects of degradation on both physicochemical and electrochemical properties have been widely studied. Key indicators of degradation include weight loss, changes in conductivity and permeability, and visible signs such as staining and cracking. For example, studies on Nafion-series membranes, such as N212, N112, N115, and N117, commonly used in VRFB applications, have revealed notable changes in their physicochemical and electrochemical properties [39-42]. These include increased water uptake, swelling ratios, and ion exchange capacity (IEC), along with visible surface changes, such as blue staining caused by VO^{2+}. Interestingly, while visible degradation is observed, the fluorinated components of Nafion membranes have shown remarkable stability. This was evidenced by ^{19}F NMR analyses, which revealed no significant differences between fresh and cycled membranes [40]. Further insights into membrane degradation mechanisms, including pore blockage by vanadium ions and functional group cleavage, have been provided by Lulay *et al.* [43]. While their review offers a comprehensive overview of membrane degradation in redox flow battery systems, detailed studies on the degradation of composite membranes in VRFBs remain limited.

This study aims to systematically evaluate the stability of N117-(PEI/GO)*n* membranes in the catholyte environment of VRFBs by analyzing key physicochemical properties, including alterations in the LbL components and changes in catholyte concentration, using Fourier-transform infrared (FTIR) and UV-visible spectroscopy, as well as measurement of weight loss, water uptake, and swelling ratio. Electrochemical properties like IEC, proton conductivity, and vanadium permeability were also examined. By elucidating the degradation mechanisms and their impact on membrane performance, this work seeks to propose strategies for enhancing membrane durability, offering critical insights for developing robust and efficient membrane technologies, particularly for LbL membranes in VRFB applications.

2. Materials and Methods

2.1. Materials

The Nafion 117 (N117) membrane, with a thickness of 180 ± 5 μm, was purchased from the Fuel Cell Store. Vanadium oxide sulfate ($VOSO_4.nH_2O$) with 97% purity and branched PEI with 50 wt.% in water and molecular weight (MW) < 100, 000 were purchased from Merck. The GO powder was obtained from Graphenea Inc.).

2.2. Membrane preparation

The membrane in this study was fabricated using a LbL modification technique as reported elsewhere [35]. In this process, polycationic PEI and polyanionic GO bilayers were sequentially deposited onto the N117 membrane, with each deposition lasting 10 min. Between each layer, the membrane was rinsed five times with deionized water to remove excess PEs. After each deposition, the membrane was thermally treated in an oven for 30 min at 60°C. This procedure resulted in the formation of N117-(PEI/GO)*n*, where '*n*' represents the number of bilayers. It should be noted that $n = 0$ denotes the pristine Nafion 117 membrane, which serves as the commercial benchmark for all comparisons in this study. Figure 1 illustrates the membrane preparation process used in this study. The physicochemical and electrochemical properties of the membranes were characterized both before and after the stability testing.

2.3. Stability test

The stability of the membranes was evaluated by immersing them for 60 days in vials containing VO_2^+ solutions under two conditions: i) normal condition, involving immersion in 0.1 M VO_2^+ in 3.0 M H_2SO_4, at ambient temperature (approximately 25 ± 3°C), and ii) accelerated (concentrated) condition, involving immersion in 1.5 M VO_2^+ in 3.0 M H_2SO_4 at 40 ± 3°C to prevent VO_2^+ precipitation. The accelerated condition was maintained at 40°C to prevent precipitation of the VO_2^+ solution. During the 60-day immersion test, the color changes in both the solutions and membranes were observed and recorded. In addition, the membrane samples were analyzed using a UV-Visible spectrophotometer (UV − 1800 Shimadzu, Japan) to identify vanadium stains and monitor changes on the membrane surfaces. The solutions from the vials were periodically sampled to determine the concentration of VO^{2+} generated using UV-Vis spectroscopy. For accurate quantification, a standard solution with various ratios of 0.1 M VO^{2+} and 0.1 M V^{5+} solutions was prepared. Furthermore, membrane weight loss and the concentration reduction of VO_2^+ to VO^{2+} of each membrane were recorded throughout the test.

2.4. Physicochemical properties

The physicochemical properties of the membranes were evaluated through various analyses, including visual observation of the membrane surfaces and examination of chemical and structural changes using FTIR spectroscopy (PerkinElmer, 4000–400 cm^{-1} wavenumber range) and Raman spectroscopy (Raman Xplora, 532 nm laser). Additionally, UV-Visible spectroscopy of the catholyte solution was performed to monitor changes in vanadium species concentration during the stability tests. Furthermore, the water uptake (WU), swelling ratio (SR), and IEC were measured. The WU and SR were determined following the procedure reported in [44,45], using the following Eqs. (1, 2), respectively.

$$WU = \frac{W_{wet} - W_{dry}}{W_{dry}} \, x100\% \tag{1}$$

$$SR = \frac{X_{wet} - X_{dry}}{X_{dry}} \, x100\% \tag{2}$$

Here, W_{wet} and X_{wet} represent the weight and thickness or length of the swollen membrane, respectively, while W_{dry} and X_{dry} denote those of the dry membrane. For the IEC determination, the membranes were first immersed in a 1.0 M sodium chloride (NaCl) solution for 24 h. The released chloride ions were then titrated with 0.01 M sodium hydroxide (NaOH), using a few drops of phenolphthalein as an indicator. The IEC value was calculated according to Eq. (3).

$$IEC = \frac{\Delta V_{NaOH} C_{NaOH}}{W_{dry}} \tag{3}$$

where ΔV_{NaOH} and C_{NaOH} are the volume (mL) and concentration of NaOH solution (M), respectively.

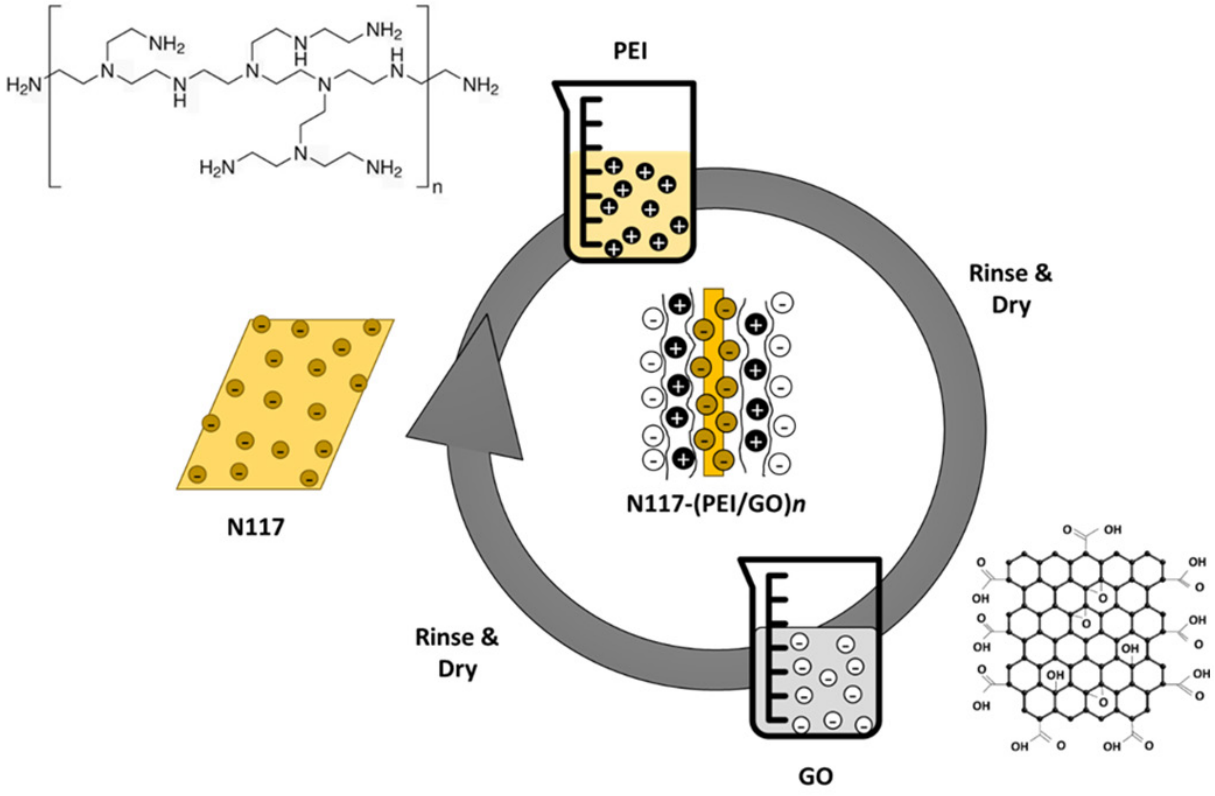

Figure 1. Schematic representation of preparation of N117-(PEI/GO)*n* using LbL modification.

2.5. Electrochemical properties

The electrochemical properties of the membranes were evaluated both before and after the stability tests. The through-plane conductivity was first measured using electrochemical impedance spectroscopy (EIS) with the MTS-740 testing device from Scribner Associates Inc. (USA). Measurements were conducted under 100% relative humidity at 30 ˚C. The proton conductivity of the membranes was calculated from the resistance (R) values obtained fromNyquist plot generated using Zplot software. The proton conductivity (σ) was determined using Eq. (4):

$$\sigma\left(\frac{S}{cm}\right) = \frac{L(cm)}{R(\Omega).A(cm^2)} \tag{4}$$

Secondly, the vanadium permeability (*P*) of the membrane was measured using vanadium ion (VO^{2+}) in a 50 cm^3 diffusion cell. The left side of the diffusion cell was filled with 1.5 M $VOSO_4$ in 3.0 M H_2SO_4, while the right side was filled with 1.5 M Na_2SO_4 in 3.0 M H_2SO_4. The membrane, with an active area of 2.0 cm^2, was placed between the two sides of the diffusion cell. Samples were periodically taken from the right side, which contained the resultant solution, and the VO^{2+} concentration was measured using a UV-visible spectrometer. The membrane selectivity was then calculated as the ratio of proton conductivity to vanadium permeability ($\sigma_{H^+}/P_{VO^{2+}}$).

3. Results and Discussion

3.1. Physicochemical properties

In general, the membranes exhibited noticeable changes in their physical appearance as the number of bilayers increased, with a gradual transition to a greyish tone, indicating successful deposition of PEI/GO. Stability testing was conducted the immersing the membranes in vanadium-containing acidic solutions to simulate operational conditions of VRFBs. To facilitate quantitative analysis, a standard calibration curve (Figure 2) was prepared by mixing varying proportions of 0.1 M VO^{2+} in 3.0 M H_2SO_4 for normal conditions and 1.5 M VO_2^+ in 3.0 M H_2SO_4 for accelerated conditions. Before the measurements, a standard curve was prepared using mixtures of 0.1 VO^{2+} and 0.1 M VO_2^+ solutions. The absorbance of each mixture was recorded at 760 nm, the wavelength at which VO^{2+} exhibited the maximum absorbance.

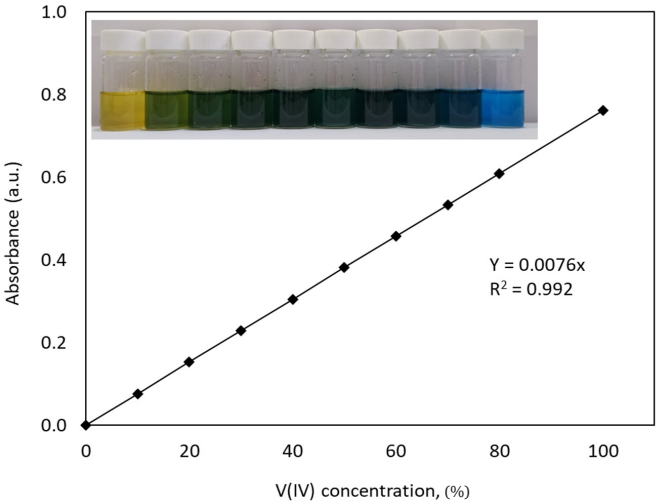

Figure 2. The absorbance of VO^{2+}/VO_2^+ solutions at different ratios at 760 nm wavelength.

In Figure 3, the membranes immersed under both normal and accelerated conditions are shown at days 0 and 60. The visual appearance reveals a noticeable decrease in color intensity over the 60-day (1440 h) period in conditions. Initially grey, the membranes gradually transition to a lighter yellowish-brown under normal conditions and to a dark bluish color under accelerated conditions. Under normal conditions, the lighter yellowish-brown coloration suggests partial penetration of the lower concentration of VO_2^+ solution into the LbL chains, leaving some

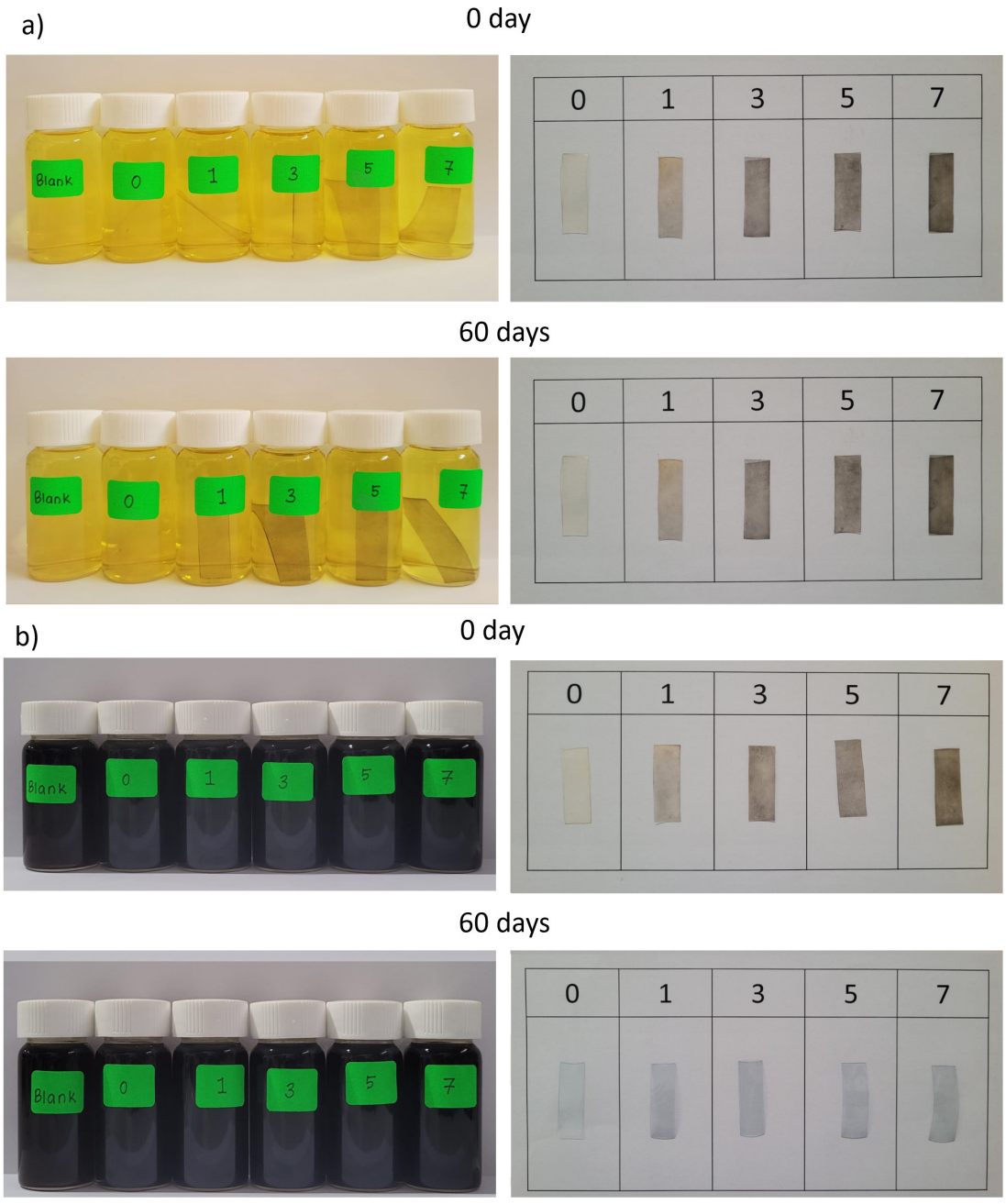

Figure 3. Figure 3. Photographs of the soaking solutions and the LbL membranes under: (a) normal and (b) accelerated conditions for 0 and 60 days of immersion.

VO_2^+ ions on the membrane surface. The accelerated conditions, on the other hand, result in a significant dark bluish color change, indicating substantial oxidation of VO_2^+ ions over time. Migration of the LbL chains within the membrane is also expected under these conditions, potentially leading to a redistribution of the VO^{2+} ions trapped in the membrane structure. Theoretically, when the membrane is oxidized by VO_2^+ ions in the solution, some VO_2^+ ions, which are yellow, are reduced to VO^{2+}, which are blue. A similar observation was reported by Kim *et al.* when using N117 under normal degradation conditions, where no apparent color change in the solutions was observed after 170 h [46]. Despite the lack of visible physical damage or significant color change in the solutions, the membranes' gradual color transition signifies an oxidative process.

The FTIR spectra revealed significant changes in the N117-(EPI/GO)*n* membranes after immersion under both normal and accelerated conditions, indicating chemical and structural modifications over time, as shown in Figure 4. Before immersion, the spectrum shows well-preserved functional groups, such as O-H, C-F, S-O, and C-H, characteristics of the pristine membrane with stable PEI and GO layers. However, after immersion under normal conditions, broadening of the O-H stretching region between 3000 – 3600 cm^{-1} suggests increased water absorption, which is supported by the slight increase in the O-H bending vibration around 1630 cm^{-1}. This indicates the presence of trapped water molecules in the membrane. Furthermore, the reduction intensity of the C=O and C=C stretching vibrations in the 1500 – 1700 cm^{-1} range hints at partial degradation of the GO layer, likely due to the interaction with VO_2^+ ions. Under accelerated conditions, these changes are even more pronounced. There is substantial broadening in the O-H stretching region, suggesting a higher degree of water uptake, along with significant reductions in the C=O and C=C peaks, indicating that GO is severely oxidized. Additionally, the C-H stretching vibrations from PEI show diminished intensity, suggesting degradation of the PEI component.

To further confirm the presence of the GO component in the LbL structure, Raman spectroscopy was conducted. Raman is particularly

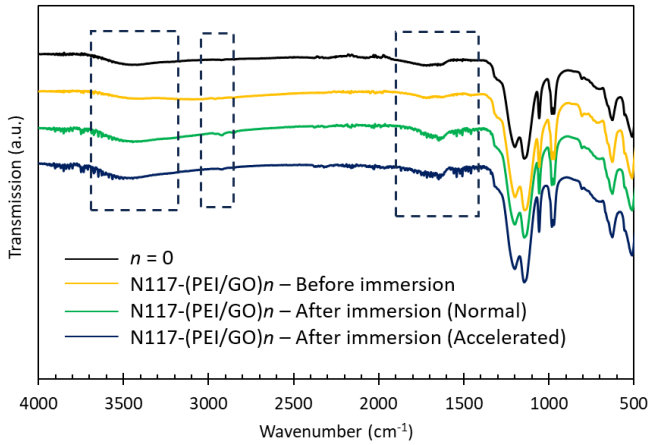

Figure 4. The FTIR of the LbL membrane before and after stability testing.

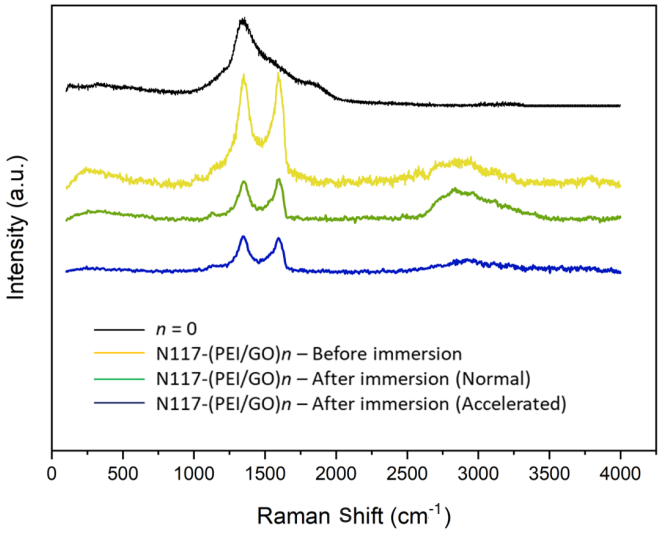

Figure 5. Raman spectroscopy for the LbL membranes before and after stability testing.

sensitive to carbon-based materials, making it an ideal tool for tracking the GO layers [47]. From Figure 5. it can be seen that the modified membranes, N117-(PEI/GO)*n* possessed prominent D and G bands at approximately 1350 cm^{-1} and 1580 cm^{-1}, respectively [48,49]. These features are absent in the pristine N117 membrane, confirming the successful deposition of GO. Furthermore, even after immersion under normal and accelerated conditions, the D and G bands remain detectable, despite minor variations in their intensity, suggesting some degree of structural alteration or degradation of the GO layers. The persistence of these bands supports the conclusion that the GO component, while partially degraded as seen in FTIR, remains structurally identifiable in the membrane system.

In addition to the visual observations and FTIR and Raman spectroscopy analysis, UV-Visible spectroscopy was employed to confirm the presence of vanadium stains within the membrane samples, as shown in Figure 6. The UV-Vis spectra reveal distinct absorbance peaks corresponding to the difference states of vanadium ions. After immersion under normal conditions, the LbL membrane shows an increase in the absorbance around 260 to 360 nm, which could be attributed to the presence of VO^{2+} ions on the membrane surface [50]. Under accelerated conditions, a notable absorbance peak appears around 760 nm, corresponding to the presence of VO_2^+ ions. These spectral changes align with the visual color transitions, where the lighter yellowish-brown color under normal conditions suggests a predominance of VO_2^+ ions, and the dark bluish color under accelerated conditions indicates a substantial reduction of VO^{2+} to VO_2^+.

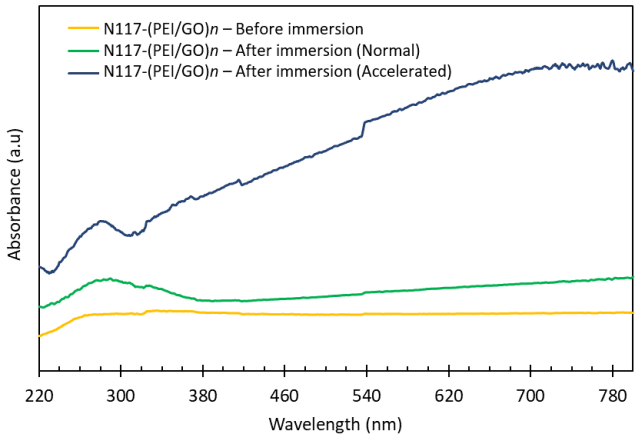

Figure 6. The UV-Vis absorption spectrum of the LbL membrane before and after stability testing.

The production of VO^{2+} ions is hypothesized to occur at a proportional rate [51]. To evaluate the degradation rate, UV-Visible spectroscopy was utilized to quantify the formation of VO^{2+} ions in solution. Figure 7 shows the changes in VO^{2+} concentration of the membrane immersed under both normal and accelerated conditions. The reported data represent normalized concentrations, considering the blank solution. When comparing the degradation of the LbL membranes, it is evident that the normal condition exhibited a significantly slower degradation rate compared to the accelerated condition. Under normal conditions, the formation of VO^{2+} ions began only after 7 days for the LbL membranes and increased gradually. In contrast, under accelerated

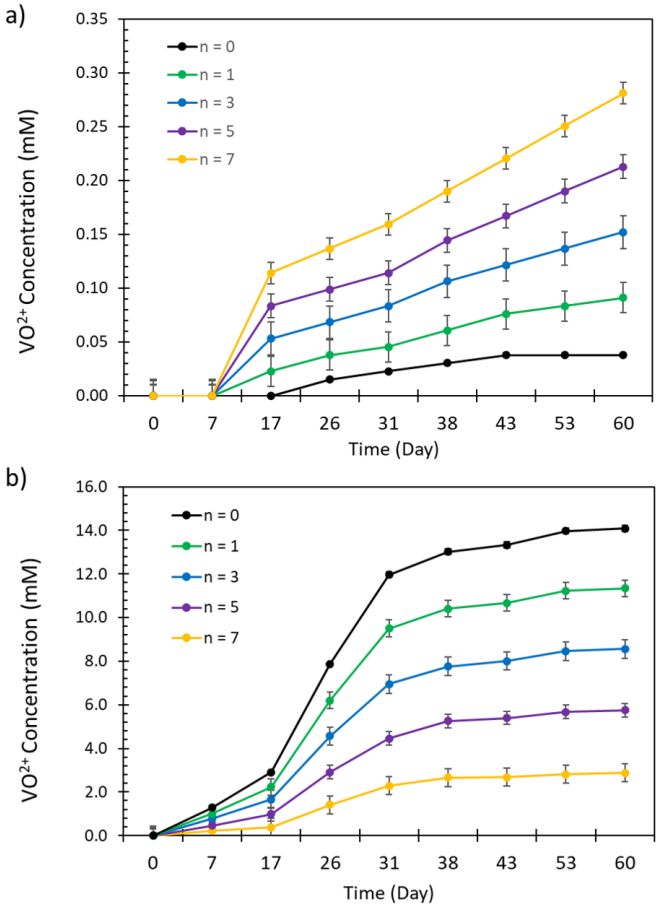

Figure 7. Changes in VO^{2+} concentration after stability test under both (a) normal and (b) accelerated conditions.

Table 1. Ex-situ chemical stability of the LbL membranes for both normal and accelerated conditions.

n	Thickness (μm)	Normal		Accelerated	
		Concentration reduction of VO_2^+ to VO^{2+} (%)	Weight loss (%)	Concentration reduction of VO_2^+ to VO^{2+} (%)	Weight loss (%)
0	180 ± 5	0.04 ± 00.1	2.1 ± 0.1	0.17 ± 0.04	4.1 ± 0.2
1	183 ± 5	0.10 ± 0.01	4.1 ± 0.2	0.37 0.03	5.6 ± 0.2
3	185 ± 6	0.16 ± 0.02	5.1 ± 0.3	0.55 ± 0.04	6.9 ± 0.3
5	213 ± 5	0.22 ± 0.02	5.4 ± 0.3	0.75 ± 0.04	8.5 ± 0.3
7	246 ± 7	0.27 ± 0.01	6.7 ± 0.4	0.93 ± 0.01	9.9 ± 0.3

conditions, the formation of VO^{2+} ions was rapid, with concentrations peaking much earlier, around 17 days.

The membrane weight loss was also measured as an indicator of the stability test. Table 1 provides a summary of the concentration reduction of VO_2^+ to VO^{2+} and the weight loss for both normal and accelerated conditions. In the case of normal degradation, the concentration reduction of VO_2^+ to VO^{2+} is lower, ranging from 0.04% to 0.27% with the lowest reduction observed for the pristine N117 membrane (n = 0). Correspondingly, the weight loss percentages are moderate, varying from 2.1% to 6.7%, increasing with the number of bilayers. In contrast, under accelerated conditions, the reduction percentages are significantly higher, between 0.17% and 0.93%, and the weight loss is more pronounced, ranging from 4.1% to 9.9%. This indicates a faster degradation rate under accelerated conditions, with higher concentration reduction of VO_2^+ to VO^{2+} and weight loss values for membranes with more bilayers. Comparing the weight loss of the pristine N117 membrane, the value obtained in this study is four times higher than the value previously reported, where the same membrane was immersed under the same conditions but shorter period, 20-30 days [52,53]. The lower the weight loss, the greater the stability of the membrane. In fact, the degradation mainly occurred in the LbL chains, as no apparent physical damages (cracking or shrinkage) were observed on the membrane. Therefore, the membrane with a higher number of bilayers experienced the highest weight loss owing to the presence of more polymer groups prone to degradation.

Figure 8 depicts the changes in WU, SR, and IEC of the membranes before and after the stability testing under both normal and accelerated conditions. In general, all membranes experienced an increase in WU and SR under both conditions. However, the increase in WU and SR of the LbL membranes is lower than that of the n = 0 membrane. This can be attributed to the acidic environment, causing structural changes in the membranes. For the n = 0 membrane, which is simpler or non-modified compared to the LbL membranes, the increase in WU and SR after the stability test was more pronounced. This greater increase can be attributed to the lack of additional layers or structural modifications that might provide resistance to the acidic conditions during the 60 days of immersion. In contrast, the LbL membranes, with their more complex structure, show a smaller increase in WU and SR. The PEI/GO bilayers in the LbL membranes provide additional stability and reduce the extent of structural degradation compared to the n = 0 membrane, leading to a comparatively smaller increase in WU and SR. The phenomenon was previously observed in N212 [51] membrane, where exposure to acidic environments led to increased WU and SR, especially in dilute solutions of 0.1 M VO_2^+, due to the lower ionic strength allowing easier penetration into the membrane pores. In addition, acidic conditions can lead to hydrolysis, resulting in higher water absorption.

The IEC of the LbL membrane increased after the stability test. The increase in IEC was more significant under accelerated conditions, with values ranging from 0.94 to 0.98 mmol·g^{-1} under normal conditions and 1.1 to 1.2 mmol·g^{-1}. The n = 0 membrane exhibited the highest IEC value for both testing conditions, as it was not surface-modified by the PEI/GO bilayers. This pattern is consistent with previous observations, such as the increase in IEC for the N112E/H^+ membrane from 1.2 mmol·g^{-1} to 3.6 mmol·g^{-1} upon exposure to VO_2^+ for 120 days [39]. The increase in IEC for these membranes is due to the presence of free SO_4^- and/or HSO_4^- ions lodging in the membrane pores and acting as co-ions in the cation exchange membrane.

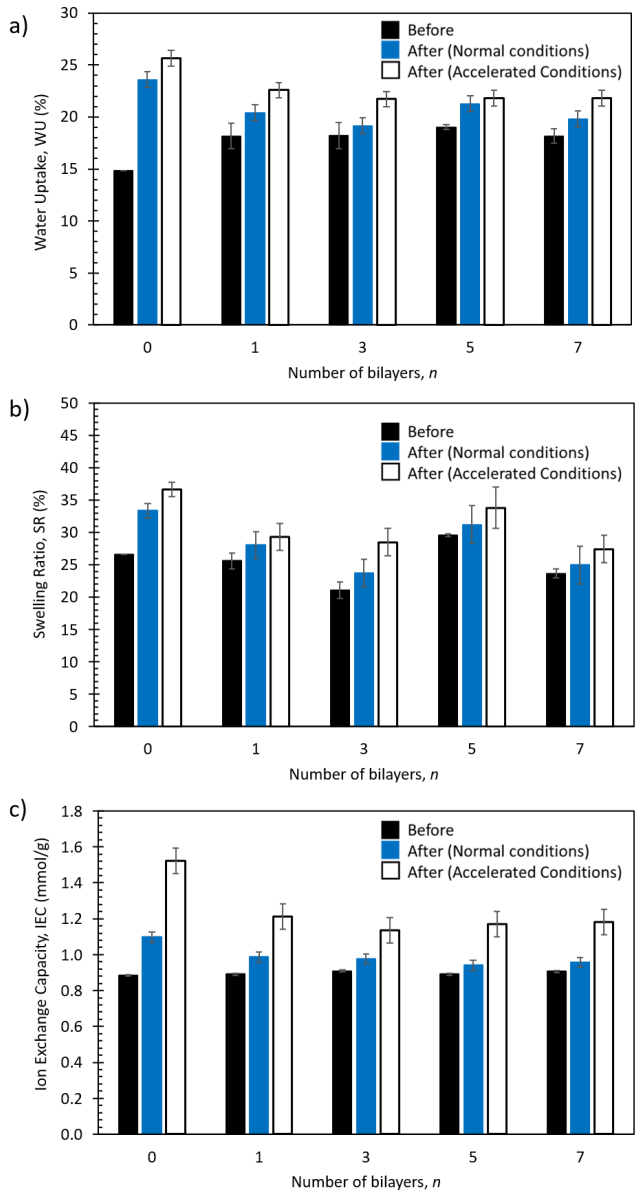

Figure 8. Values of: (a) WU, (b) SR, and (c) IEC of the membranes before and after the stability test.

The observed changes in WU and SR of the LbL membranes after the stability testing can be related to the visual changes in the immersed membranes. Under normal conditions, the transition of the membrane from grey to a lighter yellowish-brown color suggests incomplete penetration and superficial interaction with the VO_2^+ ions. This interaction leads to moderate structural changes in the membrane, reflected by the slight increases of WU, SR, and a small weight loss. Under accelerated conditions, the membranes change to a dark bluish color, indicating substantial oxidation of VO^{2+} ions. This significant oxidation implies a more aggressive interaction with the LbL chains, leading to more pronounced structural changes. These conditions promote a more extensive breakdown of the polymer structure, resulting in larger increases in weight loss, WU, and SR.

3.2. Electrochemical properties

Table 2 shows the proton conductivity, vanadium permeability, and selectivity of the membranes before and after the stability testing. These membranes were tested to investigate whether this value could adversely affect the membranes' selectivity [51]. Generally, for proton conductivity, all membranes exhibit an increase after exposure to the vanadium electrolyte. The increase ranges from 11% to 20% under

Table 2. The proton conductivity, vanadium permeability, and selectivity of the tested membranes.

n	Proton conductivity, σ (mS·cm^{-1})			Vanadium permeability, *P* (10^{-7} cm^{-2} min^{-2})			Selectivity, *S* (10^{4} S min cm^{-3})		
	Before	After (Normal)	After (Accelerated)	Before	After (Normal)	After (Accelerated)	Before	After (Normal)	After (Accelerated)
0	107.6 ± 0.2	120.1 ± 0.2	152.0 ± 0.4	74.6 ± 1.4	124.3 ± 1.5	154.3 ± 3.0	1.4 ± 0.6	1.3 ± 0.9	1.3 ± 1.8
1	97.2 ± 0.2	107.8 ± 0.2	130.1 ± 0.4	5.1 ± 0.03	15.6 ± 0.04	43.6 ± 0.04	19.2 ± 0.1	6.1 ± 0.1	3.0 ± 0.3
3	93.7 ± 0.3	112.0 ± 0.4	131.1 ± 0.2	5.1 ± 0.03	17.3 ± 0.04	41.2 ± 0.04	18.3 ± 0.2	6.5 ± 0.3	3.2 ± 0.1
5	105.1 ± 0.2	118.7 ± 0.4	130.1 ± 0.2	7.1 ± 0.05	20.5 ± 0.03	44.5 ± 0.04	14.9 ± 0.1	5.8 ± 0.3	2.9 ± 0.1
7	115.2 ± 0.4	129.4 ± 0.5	134.6 ± 0.2	11.2 ± 0.05	25.4 ± 0.08	45.0 ± 0.1	10.3 ± 0.2	4.7 ± 0.3	2.8 ± 0.1

normal conditions and from 19% to 41% under accelerated conditions. Meanwhile, there is a substantial increase in vanadium permeability across all tested membranes. The LbL membranes show an increase ranging from 127% to 762% under both conditions. In contrast, the n = 0 membrane shows a more modest increase of 30% under normal conditions and 52% under accelerated conditions. Though the range of the increment might be smaller than the LbL membranes, the vanadium permeability values of this membrane are still higher than the LbL membranes by about 74-84%. The sharp increase in vanadium permeability suggests a significant compromise in the membrane structure due to LbL degradation. Specifically, the PEI/GO bilayers, which initially contribute to the membrane's selective barrier, may break down. This degradation reduces the repulsive effects that these layers provide against proton and vanadium ions, leading to enhanced proton and vanadium transport through the membrane. Selectivity, which is a measure of the membrane's ability to preferentially allow protons over vanadium ions, decreases for all membranes after testing. The decrease is less pronounced under normal conditions but more significant under accelerated conditions. The reduction in selectivity is a direct consequence of the increases in both proton conductivity and vanadium permeability. As the membrane becomes more permeable to vanadium ions due to structural degradation, its ability to discriminate between proton and vanadium ion transport diminishes. This effect is exacerbated under accelerated conditions, which likely cause more severe degradation of the membrane structure.

3.3. LbL membrane degradation mechanism

In previous studies [27,28], the possible interactions in N117-(PEI/GO)*n* assemblies were investigated, highlighting that they primarily consist of electrostatic interactions, hydrogen bonding, and chemical bonding. Given that electrostatic interactions are the dominant force stabilizing the LbL formation, we conclude that exposure to vanadium solutions can weaken and/or disrupt these electrostatic interactions in PEI/GO LbL chains. The primary factors contributing to this degradation are changes in ionic strength, chemical reactions, oxidative effects, and complexation with PEI. These factors collectively impact the stability and integrity of the LbL assembly by modifying the electrostatic and chemical interactions between PEI and GO layers, resulting in the degradation of the modified membrane.

Moreover, the presence of highly oxidizing VO_2^+ ions and concentrated acid in the vanadium catholyte can protonate or hydrolyze the functional groups of both PEI and GO. Oxidizing agents induce chemical transformations in PEI or GO, altering their properties and weakening the interactions between the layers. Specifically, tertiary amine groups in PEI are susceptible to hydrolysis under acidic conditions. This process involves protonation of the amine group, followed by cleavage of the carbon-nitrogen bond adjacent to the protonated amine.

The amine group in PEI is particularly vulnerable to hydrolysis in highly acidic environments. In this study, branched PEI was used, which is more prone to chemical transformation compared to its linear counterpart [54]. Acidic conditions in the vanadium catholyte can catalyze the cleavage of tertiary amine bonds, leading to the breakdown of the polymer backbone and, consequently, the loss of structural integrity. Protonation attacks disrupt the electrostatic bonds between PEI and GO, as well as between PEI and the sulfonic acid groups of N117, further contributing to the destabilization of the LbL structure. When this structural integrity is compromised, GO, which is generally stable in acidic environments [55], tends to detach from the membrane due to the interfacial weakening of the composite structure.

A comparative study of LbL membranes using branched PEI and poly(allylamine hydrochloride) (PAH) as polycation for electrodialysis desalination revealed notable differences. Under the influence of the electrodialysis process, branched PEI underwent structural changes and cleavage of its tertiary amine groups after 50 hrs, leading to the breakdown of the main polymer chains. In contrast, PAH, which contains only primary amine groups, experienced cleavage that did not affect the main chains, thereby maintaining its structural integrity more effectively [54]. Figure 9 illustrates the plausible degradation mechanism of the LbL membrane in the vanadium catholyte.

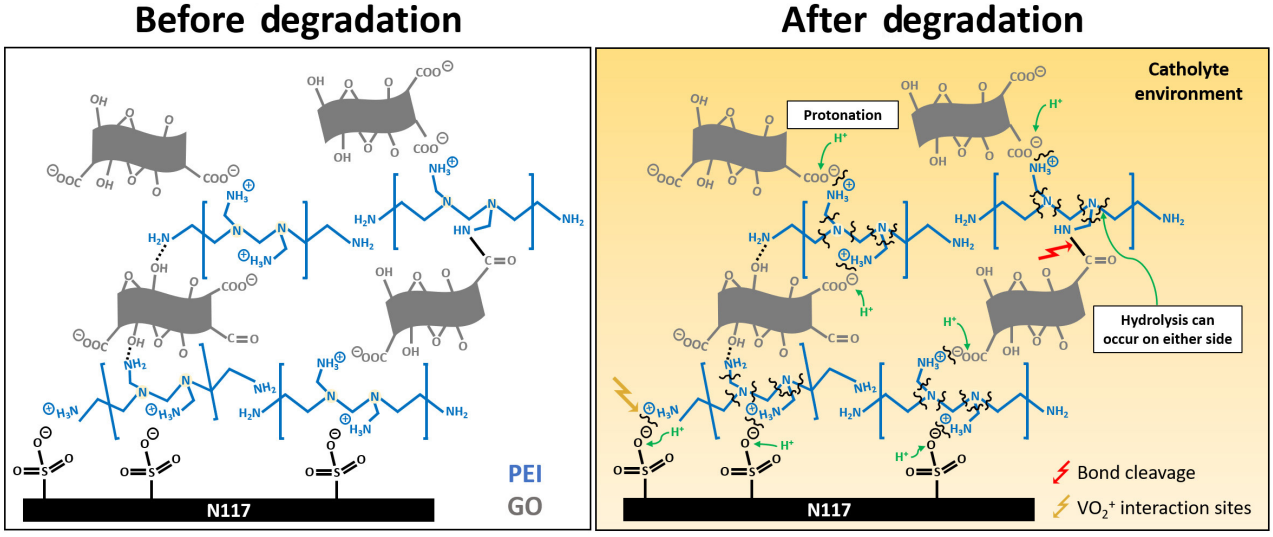

Figure 9. Degradation pathway for N117-(PEI/GO)*n* membrane in vanadium catholyte before and after testing.

Table 3. Comparison of the stabilities of various LbL membranes for VRFB application.

LbL membranes	Test conditions	Findings	References
N117-(PEI/GO)*n* and this study	In-situ: Cycling (1.65/0.8 V, 40 mA.cm^{-2}), 100 cycles Ex-situ: Immersion (0.1/1.5 M VO_2^+), 60 days	Slight reduction in VE (~4.0%) Weight loss (4.1 – 9.9%), $VO_2^+ \rightarrow VO^{2+}$ (0.1 – 0.93%) Increased proton conductivity and vanadium permeability, decreased selectivity	[35]
Nafion-NdZr-$(PDDA/PSS)_2$	In-situ: Cycling (1.70/1.0 V, 40 mA.cm^{-2}), 200 cycles Ex-situ: Immersion (1.5 M VO_2^+), 30 days	Slight reduction in efficiencies, capacity retention (73.4%) Weight loss (3.60%)	[17]
P/S-$[PDDA/PSS]_6$	In-situ: Cycling (1.65/0.8 V, 80 mA.cm^{-2}), 80 cycles	Slight reduction in VE (~4%)	[15]
Nafion-$(CS\text{-}PWA)_3$	In-situ: Cycling (1.60/0.8 V, 60 mA.cm^{-2}), 35 cycles	Slight increase in CE (~3%)	[20]
SPFEK-20.7-imidazole-$(PDDA/PSS)_8$	Ex-situ: Fenton's reagent (3 wt% H_2O_2 + 2 ppm $FeSO_4$), 1 h	Weight loss (1.14%)	[56]
SPFEK-$(PDDA/PSS)_2$	Ex-situ: Fenton's reagent (3 wt% H_2O_2 + 2 ppm $FeSO_4$), 1 h	Weight loss (1.28%)	[14]
N117-$(PDDA/PSS)_5$	In-situ: Cycling (1.65/0.8 V, 40 – 80 mA.cm^{-2}), 5 cycles for each current density	CE increased, but EE decreased with increasing current density	[13]

3.4. Stabilities of LbL membrane in VRFB environment and strategies for improvement

Table 3 tabulates the stability test conducted on various LbL membranes for VRFB applications. The data shows that the n = 1 membrane in this study, despite having a smaller number of bilayers, performs exceptionally well in terms of stability, which is crucial for VRFB applications. Its weight loss percentages are comparable to other membranes even after prolonged immersion in VO_2^+ solutions, indicating strong resistance to degradation. This performance is contrasted with other membranes, such as Nafion-NdZr-$(PDDA/PSS)_2$, which also shows good stability but under shorter immersion times [17]. Moreover, the P/S-$(PDDA/PSS)_6$ and Nafion-$(CS\text{-}PWA)_3$ membranes demonstrate slight reductions in VE and slight increases in CE, respectively, under in-situ cycling conditions, highlighting their robustness [15,20]. However, the stability under ex-situ conditions, as shown by SPFEK-based membranes exposed to Fenton's reagent, emphasizes the varying durability of different materials when subjected to oxidative environments [14]. In fact, as mentioned, in-situ cycling tests for VRFB membranes can be time-consuming due to lengthy charge/discharge processes. Therefore, while these tests are also crucial for monitoring changes in membrane properties over time, they may not immediately reveal the full extent of acidic and oxidative stability.

Overall, the comparison indicates that different membranes exhibit varying levels of stability and performance under both in-situ and ex-situ conditions. Therefore, it is crucial to comprehensively evaluate both the stability and durability of the membranes under these conditions to ensure that the membrane materials are suitable for long-term VRFB operation. Evaluation of both in-situ and ex-situ stability studies allows for a more complete understanding of how the membranes will perform over extended periods, which is essential for their practical application in VRFB systems.

There are several strategies to improve the performance and stability of LbL membranes in vanadium environments. One promising approach involves the chemical modification of PEI through the incorporation of cross-linking agents. Cross-linking strengthens the interactions between PEI and GO layers by forming covalent bonds, thereby reducing the dependence on weaker electrostatic and hydrogen bonding interactions. Common cross-linking agents, such as glutaraldehyde (GA) and epichlorohydrin (ECH), have been widely studied for various polymeric membranes [57,58]. Among these, GA is the most commonly used and well-documented crosslinker. The incorporation of cross-linking agents not only enhances membrane stability but may also improve selectivity by creating denser active layers.

Another effective strategy involves optimizing the thickness and uniformity of LbL layers. Controlled deposition methods, such as spin coating and spray-assisted assembly, can ensure consistent layer formation and minimize defects that may lead to degradation. Although these advanced deposition methods are rarely applied in VRFB membrane fabrication due to their high cost, integrating them with machine learning tools could help identify the optimal conditions [12], making the investment more feasible and valuable in the long run.

It is important to note, however, that these strategies require further exploration and validation, as most studies on LbL membranes for VRFB applications have relied on conventional fabrication methods. Future research should aim to adapt and refine these advanced techniques to effectively address the specific challenges encountered in VRFB operation.

4. Conclusions

This study highlights the significant impact of highly acidic and oxidative conditions on the stability of N117-(PEI/GO)*n* LbL-assembled membranes in VRFBs. Comprehensive stability tests revealed substantial changes in the physicochemical and electrochemical properties of the membranes, leading to the degradation of the PEI/GO bilayers. These changes include alterations in the chemical structure of the LbL assembly, variations in the vanadium catholyte concentration, and increased weight loss, water uptake, swelling ratio, IEC, proton conductivity, and vanadium permeability. The findings indicate a clear compromise in the membrane's structure and selectivity, particularly under accelerated conditions, with weight loss ranging from 4.1% to 9.9% and vanadium permeability increasing by up to 762%. The primary factor contributing to the instability of the LbL membranes is the disruption of electrostatic interactions, which are the dominant forces stabilizing the PEI/GO bilayers. Exposure to vanadium solutions weakens these interactions due to changes in ionic strength, oxidative effects, and chemical transformations. To enhance the stability and performance of LbL membranes in VRFB applications, several design improvements are proposed. These include implementing crosslinking within the LbL assemblies to improve chemical stability and optimizing the LbL deposition process through advanced methods, such as spin coating or spray-assisted assembly. The integration of machine learning tools to optimize these processes could further enhance the effectiveness of the membranes. By adopting these strategies, the design and functionality of LbL membranes can be significantly improved, ensuring greater stability and performance in VRFB applications. Future research should systematically evaluate these modifications to develop membranes capable of meeting the rigorous demands of long-term VRFB operation.

CRediT authorship contribution statement

S. S. Sha'rani: Conceptualization, Methodology, Formal analysis, Investigation, Data curation, Visualization, Writing – original draft, **E. D. M. Isa:** Formal analysis, Methodology, Validation, Visualization, Writing – review and editing, **N. F. E. N. Fadzil:** Methodology, Data curation, **M. M. Nasef:** Funding, Validation, Writing – review and editing, **E. A-Lotf:** Validation, Writing – review and editing, **N. W. C. Jusoh:** Supervision, Funding Acquisition, Project administration, Resources, Validation, Writing – review and editing.

Declaration of competing interest

The authors declare that they have no known competing financial interest or personal relationship that could have appeared to influence the work reported in this paper.

Data availability

The data will be made available on request

Declaration of generative AI and AI-assisted technologies in the writing process

The authors confirm that they have used artificial intelligence (AI)-assisted technology for assisting in the writing or editing of the manuscript or image creations.

Acknowledgment

This study was supported under the Junior Visiting Researcher scheme, Q.K130000.21A6.00P53.

References

1. Iler, R.K., 1966. Multilayers of colloidal particles. *Journal of Colloid and Interface Science*, **21**, 569-594. https://doi.org/10.1016/0095-8522(66)90018-3
2. Decher, G., 1997. Fuzzy nanoassemblies: Toward layered polymeric multicomposites. *Science*, **277**, 1232-1237. https://doi.org/10.1126/science.277.5330.1232
3. He, Y., Chen, Q.W., Yu, J.X., Qin, S.Y., Liu, W.L., Ma, Y.H., Chen, X.S., Zhang, A.Q., Zhang, X.Z., Cheng, Y.J., 2023. Yeast cell membrane-camouflaged PLGA nanoparticle platform for enhanced cancer therapy. *Journal of Controlled Release : Official Journal of the Controlled Release Society*, **359**, 347-358. https://doi.org/10.1016/j.jconrel.2023.05.043
4. Sun, B., Yang, Y., Sun, Y., Wu, D., Kan, L., Gao, C., Shi, H., Sang, C., Zhao, T., Yang, L., Ma, Q., Shi, X., 2023. Evaluating the antioxidant activity of secondary metabolites of endophytic fungi from *Hypericum perforatum* L. by an electrochemical biosensor based on AuNPs/AC@CS composite. *Bioelectrochemistry (Amsterdam, Netherlands)*, **151**, 108400. https://doi.org/10.1016/j.bioelechem.2023.108400
5. Chen, J., Xu, S., Tang, C.Y., Hu, B., Tokay, B., He, T., 2023. Stability of layer-by-layer nanofiltration membranes in highly saline streams. *Desalination*, **555**, 116520. https://doi.org/10.1016/j.desal.2023.116520
6. Yu, Y., Liu, W., Zhang, Y., Zhang, B., Jin, Y., Chen, S., Tang, S., Su, Y., Yu, X., Chen, G., 2024. Chitosan/magnetic biochar composite with enhanced reusability: Synergistic effect of functional groups and multilayer structure. *Arabian Journal of Chemistry*, **17**, 105746. https://doi.org/10.1016/j.arabjc.2024.105746
7. Fooladi, I., Ghanbarizadeh, P., Azari, A., Abbasi, M., Karami, R., Akrami, M., 2024. Titania and zirconia ceramic nanofiltration membrane fabrication by coating method on mullite and mullite-alumina microfiltration supports for industrial wastewater treatment. *Arabian Journal of Chemistry*, **17**, 105973. https://doi.org/10.1016/j.arabjc.2024.105973
8. Luo, J., Dong, C., He, R., Liu, C., He, T., 2023. Impact of support pore properties on the performance of layer-by-layer self-assembly nanofiltration membrane. *Desalination*, **557**, 116596. https://doi.org/10.1016/j.desal.2023.116596
9. Zhao, N., Platt, A., Riley, H., Qiao, R., Neagu, R., Shi, Z., 2023. Strategy towards high ion selectivity membranes for all-vanadium redox flow batteries. *Journal of Energy Storage*, **72**, 108321. https://doi.org/10.1016/j.est.2023.108321
10. Hu, X., Dong, H., Gao, N., Wang, T., He, H., Gao, X., Dai, Y., Liu, Y., Brett, D.J.L., Parkin, I.P., He, G., 2025. Self-assembled polyelectrolytes with ion-separation accelerating channels for highly stable Zn-ion batteries. *Nature Communications*, **16**, 2316. https://doi.org/10.1038/s41467-025-57666-0
11. Moghadamfar, T., López, J., Cortina, J.L., del Valle, L.J., Reig, M., 2025. Optimized ion selectivity in semiaromatic based nanofiltration membranes via PDADMAC and PSS layer-by-layer self-assembly. *Separation and Purification Technology*, **365**, 132696. https://doi.org/10.1016/j.seppur.2025.132696
12. Wang, C., Park, M.J., Yu, H., Matsuyama, H., Drioli, E., Shon, H.K., 2022. Recent advances of nanocomposite membranes using layer-by-layer assembly. *Journal of Membrane Science*, **661**, 120926. https://doi.org/10.1016/j.memsci.2022.120926
13. Xi, J., Wu, Z., Teng, X., Zhao, Y., Chen, L., Qiu, X., 2008. Self-assembled polyelectrolyte multilayer modified Nafion membrane with suppressed vanadium ion crossover for vanadium redox flow batteries. *Journal of Materials Chemistry*, **18**, 1232. https://doi.org/10.1039/b718526j
14. Wang, Y., Wang, S., Xiao, M., Han, D., Hickner, M.A., Meng, Y., 2013. Layer-by-layer self-assembly of PDDA/PSS-SPFEK composite membrane with low vanadium permeability for vanadium redox flow battery. *RSC Advances*, **3**, 15467. https://doi.org/10.1039/c3ra41670d
15. Teng, X., Yu, C., Wu, X., Dong, Y., Gao, P., Hu, H., Zhu, Y., Dai, J., 2018. PTFE/SPEEK/PDDA/PSS composite membrane for vanadium redox flow battery application. *Journal of Materials Science*, **53**, 5204-5215. https://doi.org/10.1007/s10853-017-1903-y
16. Tung, S.O., Fisher, S.L., Kotov, N.A., Thompson, L.T., 2018. Nanoporous aramid nanofibre separators for nonaqueous redox flow batteries. *Nature Communications*, **9**, 4193. https://doi.org/10.1038/s41467-018-05752-x
17. Hossain, S.I., Aziz, M.A., Shanmugam, S., 2020. Ultrahigh ion-selective and durable Nafion-NdZr composite layer membranes for all-vanadium redox flow batteries. *ACS Sustainable Chemistry & Engineering*, **8**, 1998-2007. https://doi.org/10.1021/acssuschemeng.9b06541
18. Zhang, L., Ling, L., Xiao, M., Han, D., Wang, S., Meng, Y., 2017. Effectively suppressing vanadium permeation in vanadium redox flow battery application with modified Nafion membrane with nacre-like nanoarchitectures. *Journal of Power Sources*, **352**, 111-117. https://doi.org/10.1016/j.jpowsour.2017.03.124
19. Yoo, H.Y., Heo, A., Cho, C.G., 2016. Crosslinkable layer-by-layer assembled sulfonated poly(phenylene oxide) membrane based on nafion for vanadium redox flow battery. *Journal of Nanoscience and Nanotechnology*, **16**, 10515-10519. https://doi.org/10.1166/jnn.2016.13186
20. Lu, S., Wu, C., Liang, D., Tan, Q., Xiang, Y., 2014. Layer-by-layer self-assembly of Nafion–[CS–PWA] composite membranes with suppressed vanadium ion crossover for vanadium redox flow battery applications. *RSC Advances*, **4**, 24831-24837. https://doi.org/10.1039/c4ra01775g
21. Vlasov, V.I., Gvozdik, N.A., Mokrousov, M.D., Ryazantsev, S.V., Luchkin, S.Y., Gorin, D.A., Stevenson, K.J., 2022. Ion-exchange membrane impact on preferential water transfer in all-vanadium redox flow battery. *Journal of Power Sources*, **540**, 231640. https://doi.org/10.1016/j.jpowsour.2022.231640
22. Hao, X., Chen, N., Chen, Y., Chen, D., 2022. Accelerated degradation of quaternary ammonium functionalized anion exchange membrane in catholyte of vanadium redox flow battery. *Polymer Degradation and Stability*, **197**, 109864. https://doi.org/10.1016/j.polymdegradstab.2022.109864
23. Halakoo, E., Feng, X., 2020. Self-assembled membranes from polyethylenimine and graphene oxide for pervaporation dehydration of ethylene glycol. *Journal of Membrane Science*, **616**, 118583. https://doi.org/10.1016/j.memsci.2020.118583
24. Abdolmaleki, H.R., Mousavi, S.A., Heydari, H., 2023. Novel positively charged PVDF/SPES membranes surface grafted by hyperbranched polyethyleneimine (HBPEI): Fabrication, characterization, antifouling properties, and performance on the removal of cationic E-coat paint. *Polymer Testing*, **122**, 108020. https://doi.org/10.1016/j.polymertesting.2023.108020
25. Zhang, Y., Yang, Y., Takizawa, S., Kuroda, K., Jia, Z., Liu, P., Wei, H., Graham, N.J.D., 2025. Development of a composite MoS_2/PEI nanofiltration membrane for radionuclides efficient removal from aquatic environments. *Separation and Purification Technology*, **352**, 128246. https://doi.org/10.1016/j.seppur.2024.128246
26. Ma, J., Zhen, L., Yao, H., Mo, D., Sun, Y., Hu, Z., Liu, J., Duan, J., 2025. Tunable hydrophilic modification of polyethylene terephthalate membrane via layer-by-layer polyethylenimine grafting. *Reactive and Functional Polymers*, **208**, 106151. https://doi.org/10.1016/j.reactfunctpolym.2025.106151
27. Hu, J., Yang, Z., 2022. Layer-by-layer self-assembly preparation and desalination performance of graphene oxide membrane. *Water Supply*, **22**, 126-136. https://doi.org/10.2166/ws.2021.280
28. Wang, C., Park, M.J., Gonzales, R.R., Matsuyama, H., Drioli, E., Shon, H.K., 2023. Graphene oxide-based layer-by-layer nanofiltration membrane using inkjet printing for desalination. *Desalination*, **549**, 116357. https://doi.org/10.1016/j.desal.2022.116357
29. Castillo-Ruiz, M., Negrete, C., Espinoza, J.P., Martínez, I., Daille, L.K., González, C., Rodríguez, B., 2024. Antibiofilm effects of modifying polyvinylidene fluoride membranes with polyethylenimine, poly(acrylic acid) and graphene oxide. *Polymers*, **16**, 3418. https://doi.org/10.3390/polym16233418
30. Lee, J., Kim, J., Seo, B., Shin, D., Hwang, S., Choi, W., 2023. Layer-by-layer solution-processed two-dimensional graphene oxide–polyethylenimine thin-film coatings for enhanced pool boiling heat transfer. *International Journal of Heat and Mass Transfer*, **209**, 124067. https://doi.org/10.1016/j.ijheatmasstransfer.2023.124067
31. Palen, B., Iverson, E.T., Rabaey, M.G., Kulatilaka, S., Grunlan, J.C., 2023. Graphene oxide nanobrick wall for gas barrier and fire protection of polystyrene. *Journal of Materials Science*, **58**, 7594-7601. https://doi.org/10.1007/s10853-023-08491-7
32. Li, P., Yu, M., Gao, K., Chen, K., Yang, X., Sun, H., Hou, Y., Niu, Q.J., 2023. Rapid preparation of hydrogen barrier films by a novel ultrasonic atomization-assisted layer-by-layer self-assembly method. *International Journal of Hydrogen Energy*, **48**, 25783-25796. https://doi.org/10.1016/j.ijhydene.2023.03.273
33. Baruah, K., Nandi, S., M., P., K., R., S., R., Deb, P., 2024. A versatile non-precious metal based electrode material endowed by layer-on-layer structure for methanol oxidation and supercapacitor applications. *Journal of Energy Storage*, **84**, 110867. https://doi.org/10.1016/j.est.2024.110867
34. Wang, L., Wang, N., Yang, H., An, Q., Zeng, T., Ji, S., 2018. Enhanced pH and oxidant resistance of polyelectrolyte multilayers via the confinement effect of lamellar graphene oxide nanosheets. *Separation and Purification Technology*, **193**, 274-282. https://doi.org/10.1016/j.seppur.2017.10.061
35. S'rani, S.S., Nasef, M.M., Jusoh, N.W.C., Isa, E.D.M., Ali, R.R., 2024. A highly-selective layer-by-layer membrane modified with polyethylenimine and graphene oxide for vanadium redox flow battery. *Science and Technology of Advanced Materials*, **25**, 2300697. https://doi.org/10.1080/14686996.2023.2300697
36. Tang, W., Leng, S., Jin, Y., Liu, R., Che, X., Liu, J., Yang, J., 2021. New crosslinked membranes based on cardo-poly(etherketone) and poly(ethylene imine) for the vanadium redox flow battery. *European Polymer Journal*, **161**, 110858. https://doi.org/10.1016/j.eurpolymj.2021.110858
37. Balaji, J., Sethuraman, M.G., Roh, S.H., Jung, H.Y., 2020. Recent developments in sol-gel based polymer electrolyte membranes for vanadium redox flow batteries – A review. *Polymer Testing*, **89**, 106567. https://doi.org/10.1016/j.polymertesting.2020.106567
38. Guo, Y., Huang, J., Feng, J.K., 2023. Research progress in preparation of electrolyte for all-vanadium redox flow battery. *Journal of Industrial and Engineering Chemistry*, **118**, 33-43. https://doi.org/10.1016/j.jiec.2022.11.037
39. Sukkar, T., Skyllas-Kazacos, M., 2004. Membrane stability studies for vanadium redox cell applications. *Journal of Applied Electrochemistry*, **34**, 137-145. https://doi.org/10.1023/b:jach.0000009931.83368.dc
40. Vijayakumar, M., Bhuvaneswari, M.S., Nachimuthu, P., Schwenzer, B., Kim, S., Yang, Z., Liu, J., Graff, G.L., Thevuthasan, S., Hu, J., 2011. Spectroscopic investigations of the fouling process on Nafion membranes in vanadium redox flow batteries. *Journal of Membrane Science*, **366**, 325-334. https://doi.org/10.1016/j.memsci.2010.10.018

41. Xi, J., Jiang, B., Yu, L., Liu, L., 2017. Membrane evaluation for vanadium flow batteries in a temperature range of −20–50°C. *Journal of Membrane Science*, **522**, 45-55. https://doi.org/10.1016/j.memsci.2016.09.012
42. Mukherjee, S., Kayal, P., Das, S., Raja, M.W., 2025. Sustainable paper based cellulose nano-crystal (CNC) impregnated flexible ion exchange membrane (IEM) for vanadium redox flow batteries (VRFBs). *Materials Research Bulletin*, **188**, 113413. https://doi.org/10.1016/j.materresbull.2025.113413
43. Lulay, F., Weidlich, C., Valtiner, M., Pichler, C.M., 2023. Membrane degradation in redox flow batteries. *Green Chemistry Letters and Reviews*, **16**, 1-15. https://doi.org/10.1080/17518253.2023.2274529
44. Thiam, B.G., Vaudreuil, S., 2021. Review—Recent membranes for vanadium redox flow batteries. *Journal of The Electrochemical Society*, **168**, 070553. https://doi.org/10.1149/1945-7111/ac163c
45. Doan, T.N.L., Hoang, T.K.A., Chen, P., 2015. Recent development of polymer membranes as separators for all-vanadium redox flow batteries. *RSC Advances*, **5**, 72805-72815. https://doi.org/10.1039/c5ra05914c
46. Kim, S., Tighe, T.B., Schwenzer, B., Yan, J., Zhang, J., Liu, J., Yang, Z., Hickner, M.A., 2011. Chemical and mechanical degradation of sulfonated poly(sulfone) membranes in vanadium redox flow batteries. *Journal of Applied Electrochemistry*, **41**, 1201-1213. https://doi.org/10.1007/s10800-011-0313-0
47. Waghmare, Y.A., Ingle, N.N., Tsai, M.L., Hianik, T., Shirsat, M.D., 2025. Highly selective and sensitive chemiresistive NO_2 sensor using reduced graphene oxide/metal-base porphyrin composite. *Sensors and Actuators A: Physical*, **391**, 116628. https://doi.org/10.1016/j.sna.2025.116628
48. Guo, J., Pei, S., Huang, K., Zhang, Q., Zhou, X., Tong, J., Liu, Z., Cheng, H.M., Ren, W., 2025. Control of water for high-yield and low-cost sustainable electrochemical synthesis of uniform monolayer graphene oxide. *Nature Communications*, **16**, 727. https://doi.org/10.1038/s41467-025-56121-4
49. Tripathi, S., Gangwar, N., Gangwar, C., Shukla, R.K., 2025. Enhanced humidity sensing using graphene oxide and reduced graphene oxide synthesized via modified hummers' method. *Sensing and Imaging*, **26**, 1-20. https://doi.org/10.1007/s11220-025-00547-z
50. Alghool, S., Abd El-Halim, H.F., Mostafa, A.M., 2019. an eco-friendly synthesis of V_2O_5 nanoparticles and their catalytic activity for the degradation of 4-nitrophrnol. *Journal of Inorganic and Organometallic Polymers and Materials*, **29**, 1324-1330. https://doi.org/10.1007/s10904-019-01096-1
51. Zhao, N., Riley, H., Song, C., Jiang, Z., Tsay, K.C., Neagu, R., Shi, Z., 2021. Ex-situ evaluation of commercial polymer membranes for vanadium redox flow batteries (VRFBs). *Polymers*, **13**, 926. https://doi.org/10.3390/polym13060926
52. Sheng, J., Li, L., Wang, H., Zhang, L., Jiang, S., Shi, H., 2023. An ultrahigh conductivity and efficiency of SPEEK-based hybrid proton exchange membrane containing amphoteric GO-VIPS nanofillers for vanadium flow battery. *Journal of Membrane Science*, **669**, 121326. https://doi.org/10.1016/j.memsci.2022.121326
53. Zhang, Y., Wang, H., Qian, P., Zhou, Y., Shi, J., Shi, H., 2020. Sulfonated poly(ether ether ketone)/amine-functionalized graphene oxide hybrid membrane with various chain lengths for vanadium redox flow battery: A comparative study. *Journal of Membrane Science*, **610**, 118232. https://doi.org/10.1016/j.memsci.2020.118232
54. Solonchenko, K., Rybalkina, O., Chuprynina, D., Kirichenko, E., Kirichenko, K., Nikonenko, V., 2022. Stability of properties of layer-by-layer coated membranes under passage of electric current. *Polymers*, **14**, 5172. https://doi.org/10.3390/polym14235172
55. Sharma, J., Kulshrestha, V., 2023. Advancements in polyelectrolyte membrane designs for vanadium redox flow battery (VRFB). *Results in Chemistry*, **5**, 100892. https://doi.org/10.1016/j.rechem.2023.100892
56. Wang, Y., Wang, S., Xiao, M., Han, D., Meng, Y., 2014. Preparation and characterization of a novel layer-by-layer porous composite membrane for vanadium redox flow battery (VRB) applications. *International Journal of Hydrogen Energy*, **39**, 16088-16095. https://doi.org/10.1016/j.ijhydene.2014.02.100
57. Wang, C., Park, M.J., Gonzales, R.R., Phuntsho, S., Matsuyama, H., Drioli, E., Shon, H.K., 2022. Novel organic solvent nanofiltration membrane based on inkjet printing-assisted layer-by-layer assembly. *Journal of Membrane Science*, **655**, 120582. https://doi.org/10.1016/j.memsci.2022.120582
58. Liu, C., Shi, L., Wang, R., 2015. Crosslinked layer-by-layer polyelectrolyte nanofiltration hollow fiber membrane for low-pressure water softening with the presence of SO_4^{2-} in feed water. *Journal of Membrane Science*, **486**, 169-176. https://doi.org/10.1016/j.memsci.2015.03.050